Decomposed defect formation energy for analysis of doping process: The case of n-type and p-type doping of β-FeSi$_2$

View Online   Export Citation   CrossMark

Jun Chai,[1,2,a] (ID) Chen Ming,[2] (ID) and Yi-Yang Sun[2,a] (ID)

AFFILIATIONS

[1]College of Chemical and Material Engineering, Quzhou University, Quzhou 324000, Zhejiang, China
[2]State Key Laboratory of High Performance Ceramics and Superfine Microstructure, Shanghai Institute of Ceramics,
 Chinese Academy of Sciences, Shanghai 201899, China

[a]Authors to whom correspondence should be addressed: chaijun@qzc.edu.cn and yysun@mail.sic.ac.cn

ABSTRACT

Defect formation energy governs the thermodynamics of a specific dopant within the host material. Here, we introduce an approach to decomposing the defect formation energy into intuitive components, each representing a distinct physical step in the process of defect formation. Through this approach, we illustrate that adhering solely to conventional criteria, such as ionic radius, may overlook potential dopants. Taking β-FeSi$_2$, a promising high-temperature thermoelectric material, as an example, we demonstrate that non-intuitive chemical interactions can play a more significant role in lowering the defect formation energy. As a result, Ir on Fe site is found to exhibit unexpected low defect formation energy among the 26 candidate dopants and has been employed in experiment to enhance the thermoelectric figure of merit of n-type β-FeSi$_2$. The understanding gained from this work could be of general interest for addressing the doping limit issue for other potential thermoelectric materials.

Semiconductors play a critical role in the development of the modern electronics industry, as they are essential in the design and manufacture of electronic devices, such as transistors, diodes, and integrated circuits (IC).[1–7] Various defects in semiconductors make their electronic properties different from those of insulators. Doping is a common way to induce the defects that can govern the transport properties of semiconductors, such as the conductivity type, carrier concentration, and mobility, ultimately enhancing or compromising the performance of the hosts.[8,9] β-FeSi$_2$, a silicide semiconductor with an optical bandgap of 0.80–0.87 eV, has been investigated for decades as a traditional thermoelectric (TE) material.[10–12] However, its practical application is restricted by the low figure of merit zT as given by $zT = S^2 \sigma T / \kappa$, where S, σ, κ, and T refer to the Seebeck coefficient, electrical conductivity, thermal conductivity, and absolute temperature, respectively.[13–15] Doping is a common strategy to improve the zT of β-FeSi$_2$. Co, Mn, Al, and Ir are currently the optimal elements among the reported dopants.[16–23]

TE materials usually require heavy doping to reach the optimal carrier concentration for peak zT. For this purpose, both doping efficiency and doping concentration need to be increased. The doping

efficiency is related to the defect activation energy as studied in our previous work.[24] The doping concentration is determined by the miscibility (or solubility) of a particular element in the β-FeSi$_2$ lattice from a microscopic point of view. Therefore, it is important to evaluate the defect formation energy of dopants as it is related to the doping limit. Our previous study by density functional theory (DFT) calculations identified Ir as a heavy dopant in β-FeSi$_2$, which has been verified by experiment.[19] To further develop this material toward practical applications, it is desirable to understand the mechanism behind the high solubility of some elements such as Ir.

In this paper, using DFT-based first-principles calculations, we systematically study the defect formation energies of 26 candidate dopants (both n-type and p-type) in β-FeSi$_2$. Up to 235 secondary phases are fully considered to determine the allowed regions of the chemical potentials of dopant elements. With the obtained dataset, we propose a scheme to decompose the defect formation energy, which includes the energy of creating a vacancy, the energies of relaxing the surrounding atoms, the binding energy of the dopant atom at the vacancy site, and the atomic chemical potential. Such a decomposition scheme allows us to analyze the origin when an attractive candidate exhibits abnormally

30 December 2023 08:25:46

low formation energy. The analysis could help design the doping strategy toward optimal dopant concentration and, in turn, enhanced materials property.

The defect formation energy calculations were based on DFT with the generalized gradient approximation of Perdew–Burke–Ernzerhof (PBE)[25] for the exchange–correlation functional, as implemented in the Vienna *ab initio* simulation package (VASP).[26] The projector augmented wave (PAW) potentials were used to describe the core–valence interaction.[27] The cutoff energy for the plane wave basis was set to be 40 Ry. A 96-atom supercell was employed to model the defects. A $3 \times 3 \times 3$ k-point grid[28] was used to sample the Brillouin zone. All calculations were spin-polarized.

The formation energy of a point defect (E_{form}) is calculated by[29–32]

$$E_{form} = E_{defect} - E_{perfect} + \left(E_{Fe/Si} + \mu_{Fe/Si}\right) - \left(E_D + \mu_D\right), \quad (1)$$

where E_{defect} and $E_{perfect}$ are the total energy of the defect-containing and defect-free supercell, respectively. μ_X is the chemical potential with respect to the reference energy E_X, which is the total energy per atom of Fe, Si, or a dopant element (denoted by D) in its stable phase. The allowed region for chemical potentials is determined by the existence of all possible secondary phases (i.e., other Fe–Si compounds, D–Si compounds, and Fe–D compounds). In the supplementary material, Fig. S1 shows the relative stability of the secondary phases for each system, and Table S1 lists all the secondary phases considered in our calculations. Note that we consider neutral charge state only in this work. Thermoelectric materials are typically heavily doped semiconductors, and the Fermi level is very close to the band edges. In such cases, regardless of a deep or shallow defect, the neutral charge state possesses the lowest formation erergy of the defect.

For the $3d$ transition metal (TM) elements, adding Hubbard U[33] could improve the description on the localized electronic orbitals. However, it is not straightforward to apply the Hubbard U in defect formation energy calculations, which require to use identical U values when calculating the total energy of the defect supercell and the chemical potential of the TM dopant. The U values for $3d$ TM in their elemental phases are usually small (about 1 eV),[34] while in the β-FeSi$_2$ lattice, an appropriate U value is required. Also, the same TM element in different valence states may also require different U values.[35] Given this uncertainty, we did not include the Hubbard U correction in this work. In Fig. S2 in the supplementary material, we assessed the possible errors due to the exclusion of the Hubbard U effect by calculating the formation energies with different U values for Co, Ni, and Cu, which are expected to exhibit large U values. As the result shows, the errors are about 0.1–0.3 eV. We also evaluated the effect of spin–orbit coupling (SOC) on the formation energies. We considered Ir (a key dopant element studied in this work) and Au (the heaviest dopant element in this work, which exhibits the strongest SOC) on the Fe-site. Our results show that the formation energies with and without the SOC correction differ by 0.05 and 0.08 eV for the case of Ir and Au, respectively, which are small enough to be neglected for the purpose of this work.

Thermoelectric materials are typically heavily doped semiconductors. So, the Fermi level is close to the band edges. Taking p-type doping as an example, it can be seen that regardless of deep or shallow acceptors and irrespective of the charge state, the neutral charge state possesses the lowest Eform. For n-type doping, the case is similar. Therefore, in this work, we mainly consider the neutral charge state.

β-FeSi$_2$ crystallizes in a base-centered orthorhombic *Cmca* space group (No. 64), as shown in Fig. S3. The conventional unit cell has 48 atoms, and the experimental lattice constants are $a = 9.863$ Å, $b = 7.791$ Å, and $c = 7.833$ Å.[36] There are two inequivalent Fe-sites (Fe1-8d and Fe2-8f) and two inequivalent Si-sites (Si1-16g and Si2-16g). These inequivalent sites were all considered when calculating the E_{form}. Below, we only present the lowest E_{form} for each type of element.

We calculated the E_{form} of 18 TM elements located three columns to the left and right of Fe in the periodic table for Fe-site doping, and eight main-group elements located one column to the left and right of Si for Si-site doping. Totally, 26 candidate dopants were calculated. In order to obtain reliable E_{form}, we have considered 235 secondary phases. Automated high-throughput calculations were employed to generate the inputs and analyze the results. Table S1 lists all the possible secondary phases of the Fe–Si–D system. The enthalpy of formation of these phases with respect to bulk Fe, Si, and D was calculated and shown in Fig. S1. These data were used to evaluate the allowed region for the chemical potentials of Fe, Si, and D.

As shown in the lower panels of Figs. 1(a) and 1(b), E_{form} of Co and Ir is among the lowest in the 13 possible n-type dopants, and E_{form} of Mn and Al is among the lowest in the 13 possible p-type dopants. These results are consistent with existing experiments that Co, Ir, Mn, and Al have the highest dopant concentrations limit in FeSi$_2$ among all reported n-type and p-type dopants.[18–20,37–39] It is worthwhile noting that P also has a relatively low E_{form}. However, experimental work suggests that P doping is prone to volatilization,[40] which leads to a low solubility limit in β-FeSi$_2$.

To better understand the effect of secondary phases on E_{form}, we separated this part of contribution out and referred to it as E_μ, as shown in the upper panel of Figs. 1(a) and 1(b). We found that E_μ can be either positive or negative, which mainly depends on the formation enthalpy of the secondary phases. For the doping of Rh and N, the formation enthalpy of the secondary phases Rh$_3$Si$_4$ and Si$_3$N$_4$ is extremely low, and the condition of μ_{Rh} and μ_N used for calculating E_{form} is lower than -3.5 eV as seen in Fig. 2, which suggests that they are easily formed during doping. Therefore, E_{form} is significantly elevated, and the doping limit will be lowered. These results are different from the previous study without considering the secondary phases.[19]

On the other hand, for the doping of Cu, the formation enthalpy of the secondary phases Cu$_{15}$Si$_4$ is high, and the condition of μ_{Cu} used for calculating E_{form} is higher than -0.1 eV, as seen in Fig. S1. Moreover, the doping of Ag and Au will not form the secondary phases. Therefore, the E_{form} of Cu, Ag, and Au is greatly lowered. Nevertheless, the E_{form} of these elements is still high. For the remaining dopants, as shown in Fig. S1, the condition of chemical potential of dopant elements (μ_D) used for calculating E_{form} is close to μ_{Fe} for Fe-site doping (or μ_{Si} for Si-site doping). Thus, they cancel out during the calculation, so the secondary phases have almost nearly no contribution to E_{form}.

To gain further insights into the calculated E_{form}, we decomposed the doping process into four steps and obtained four corresponding energies. Below we take Fe-site doping as example to discuss this decomposition scheme. The four steps are as follows:

(1) The first step is to remove an Fe atom from a perfect supercell to form a Fe vacancy without relaxing the surrounding atoms. The energy change of this part is termed as vacancy energy (E_v), which is calculated by
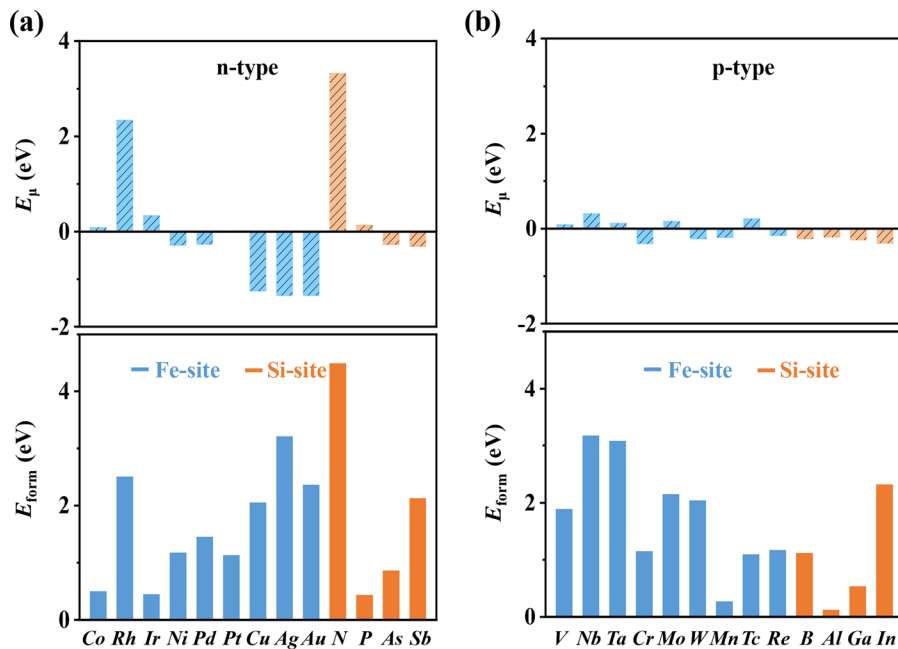
FIG. 1. Calculated defect formation energy (E_{form}) of 13 n-type dopants (a) and 13 p-type dopants (b) in β-FeSi$_2$ (the lower panels). The upper panels show the contribution of secondary phases (E_μ) to E_{form}. All E_{form}s are the lowest under the allowed chemical potential regions.

$$E_v = E_{v_{Fe}}^{unrelaxed} + E_{Fe} - E_{perfect}, \qquad (2)$$

where $E_{v_{Fe}}^{unrelaxed}$ is the total tenergy of the supercell containing the Fe vacancy but without relaxation, E_{Fe} is the total energy per atom of Fe in the *bcc* phase, and $E_{perfect}$ carries the same meaning as in Eq. (1).

(2) The second step is the relaxation of the surrounding atoms to reach the lowest energy, and the energy change of this part is termed as relaxation energy (E_r), which is calculated by

$$E_r = E_{v_{Fe}}^{relaxed} - E_{v_{Fe}}^{unrelaxed}, \qquad (3)$$

where $E_{v_{Fe}}^{relaxed}$ is the total energy of the supercell after relaxing the surrounding atoms of the Fe vacancy.

(3) The third step is to distort the atomic structure of the Fe vacancy defect to accommodate the dopant D atom. The energy change of this part is termed as distortion energy (E_d), which is calculated by

$$E_d = E_{v_D}^{relaxed} - E_{v_{Fe}}^{relaxed}, \qquad (4)$$

where $E_{v_D}^{relaxed}$ is obtained by further relaxing the supercell containing the Fe vacancy by assuming that the surrounding atoms are located at the lowest energy positions when inserting the D atom at the Fe vacancy.

(4) The fourth step is to insert the dopant D atom to the Fe vacancy site. The energy change of this part is termed as binding energy (E_b), which is calculated by

$$E_b = E_{defect} - E_{v_D}^{relaxed} - E_D, \qquad (5)$$

where E_D is the total energy per atom of D in its most stable phase and E_{defect} carries the same meaning as in Eq. (1).

The contribution of secondary phases to E_{form} is included by E_μ, and $E_\mu = \mu_{Fe} - \mu_D$ in Fe-site doping. Based on the aforementioned decomposition scheme, E_{form} of Fe-site dopants can be written as
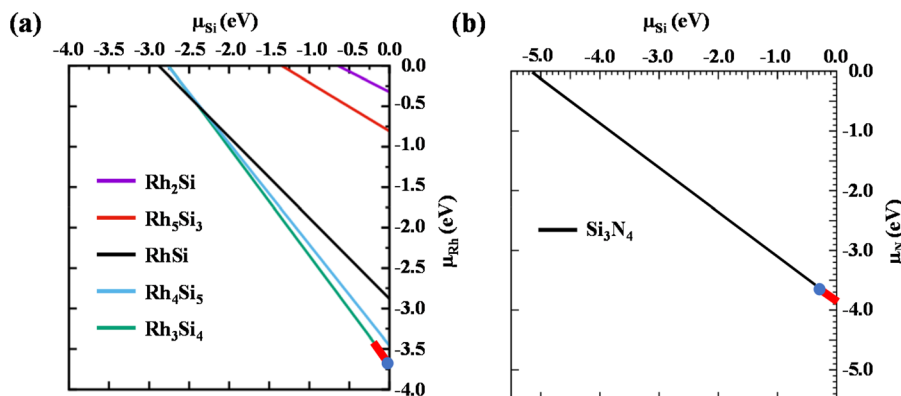
FIG. 2. Calculated stable region of β-FeSi$_2$ in the chemical potential space spanned by (a) μ_{Si} and μ_{Rh} and (b) μ_{Si} and μ_N, where the thick red segments mark the allowed chemical potential regions and the blue dots indicate the conditions used for calculating E_{form} of Rh and N, at which the corresponding E_{form} is the lowest.
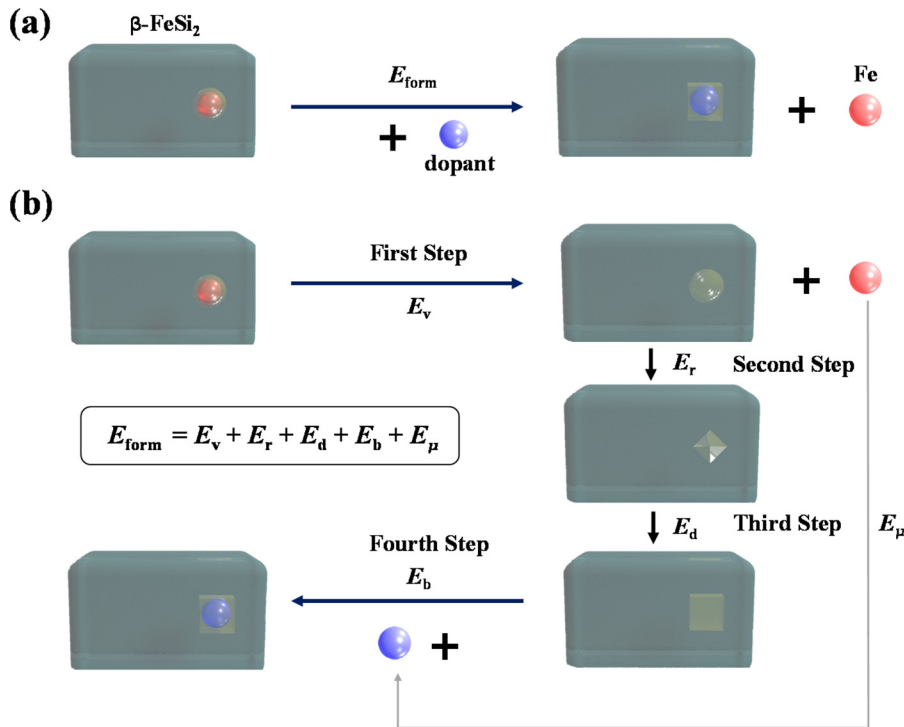
FIG. 3. (a) Schematic showing the process of introducing a dopant in β-FeSi$_2$. (b) Decomposition of the doping process into four steps and the four corresponding energies are termed as E_v, E_r, E_d, and E_b. The energy contribution of secondary phases to E_{form} is represented by E_μ, corresponding to Fig. 1, and it is calculated as the difference between μ_D and μ_{Fe} (or μ_{Si}). The defect formation energy E_{form} is equal to the sum of E_v, E_r, E_d, E_b, and E_μ.

$$E_{form} = E_v + E_r + E_d + E_b + E_\mu$$
$$= E_{defect} - E_{perfect} + (E_{Fe} + \mu_{Fe}) - (E_D + \mu_D), \quad (6)$$

which is the same as Eq. (1).

The schematics for the overall doping process and the decomposed processes are shown in Fig. 3. E_v and E_r are constants independent of the dopants. E_d reflects the extent of lattice distortion caused by the dopant atom, while E_b represents the interaction between the dopant atom and its surrounding Si atoms. To determine E_d, it is necessary to insert the dopant atom at the vacancy site and fully relax the structure. Then, the dopant atom is removed, and the total energy difference before and after this relaxation is defined as E_d. Therefore, in addition to the contribution by secondary phases (i.e., E_μ), as discussed earlier, E_{form} is also determined by E_d and E_b. Next, we analyze the behavior and trend of these two terms.

We first investigated the relationship between E_d and the magnitude of the distortion (denoted as d). To obtain the values of d, we inserted the corresponding atoms at the Fe vacancy site, which has been relaxed for calculating E_r, measured the distances between the dopant atom and the eight neighboring Si atoms, and then took the average as d. As shown in Fig. 4, E_d and d^2 are approximately linearly related. We therefore conclude that the distortion energy E_d is dominated by elastic energy, which scales as the square of d.

Figure 5 shows the trend for the binding energy (E_b) of the TM dopants at the Fe sites. For the TM dopants on the same row of the periodic table, the closer to the Fe-group, the lower the E_b. Thus, the E_b follows a V-shape trend. As we considered neutral dopant defects here, for the case of donors, the more extra electrons occupying the conduction band (i.e., the further away from the Fe-group on the periodic table), the higher the system energy is. Similarly, for the case of

acceptors, the more holes occupying the valence band, the higher the system energy is. Thus, the V-shape trend can be understood. For the same group of dopants, the acceptors and donors behave oppositely in terms of E_b. For the case of acceptors, the smaller the atomic number, the lower the E_b, while for the case of donors, the greater the atomic number, the lower the E_b. This can be attributed to an argument based on the Coulombic interaction. 5d-TM dopants are more prone to lose or gain electrons from β-FeSi$_2$ matrix than 3d-TM dopants as 5d
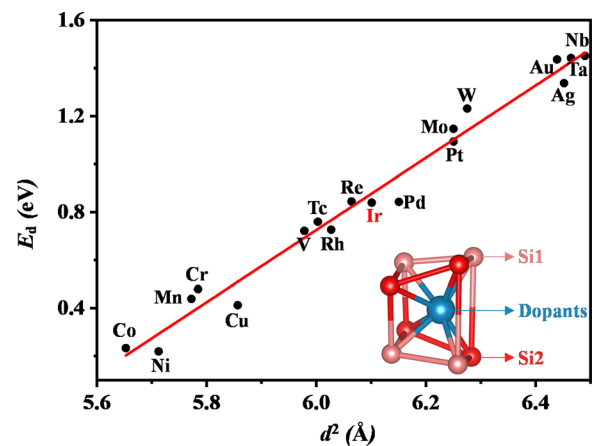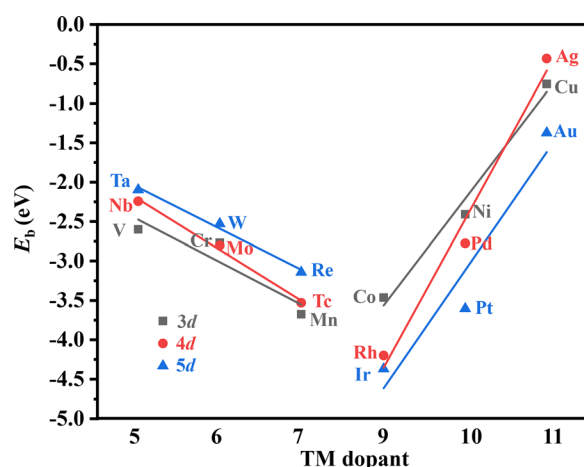

FIG. 4. Energy change caused by lattice distortion (E_d) as a function of d^2 of 18 TM dopants in β-FeSi$_2$. The red line is the linear fitting of E_d and d^2. The inset shows the dopant atom encompassed by eight Si atoms, and the d is defined by the average of the eight Si-dopant bonds.

FIG. 5. Binding energy (E_b) of 18 TM dopants in β-FeSi$_2$. The black, red, and blue lines are the linear fitting of E_b for 3d, 4d, and 5d TM dopants.

orbital is more delocalized than $3d$ orbital. Therefore, considering that the dopant is neighboring to the negatively charged Si ions, the more positively charged donor defect (e.g., $5d$ donors) will yield a stronger binding (e.g., the case of Ir on Fe-site). Similarly, the more negatively charged acceptor defect (e.g., $5d$ acceptors) will yield a weak binding (e.g., the case of Ta on Fe-site) because of the repulsive Coulombic interaction. Thus, we can qualitatively understand the trend from 3d, 4d, to 5d dopants.

Our results reveal that the binding energy E_b has a significant impact on the defect formation energy E_{form}. In particular, consider the case of Co and Ir. Intuitively, one might expect Co to have a lower E_{form} than Ir, given that Ir has a larger atomic radius and, consequently, a larger distortion energy (E_d) than Co, as shown in Fig. 4. However, Ir actually exhibits even lower E_{form} than Co by 52 meV. This is primarily due to Ir having a significantly lower E_b compared to Co.

Taking β-FeSi$_2$ as a representative thermoelectric material that requires heavy doping for tuning the electronic properties, we performed a systematic study on the defect formation energy (E_{form}) of 26 dopants in β-FeSi$_2$ based on first-principles calculations. To obtain conclusive results, we considered totally 235 secondary phases to determine the allowed regions of the elemental chemical potentials. With these results, we carried out a decomposition analysis to understand the trend of the calculated defect formation energies. By decomposing the doping process into four distinct parts, we found that E_{form} for doping on the same lattice site is determined by E_μ, E_d, and E_b, where E_μ indicates the contribution due to the secondary phases, E_d represents the elastic energy due to the local distortion, and E_b is the binding energy between the dopant and neighboring ions. It is the last term (i.e., E_b) that renders Ir to have an unexpected low E_{form}, which has been experimentally explored to fabricate the highest efficiency β-FeSi$_2$ thermoelectric devices. The method presented here is expected to be generally applicable to the optimization of other thermoelectric materials by dopant engineering.

See the supplementary material for the determination of the allowed region for chemical potentials, the correlation between E_{form} and U, the crystal structure of β-FeSi$_2$, and binary compounds of Fe–Si–D systems.

AUTHOR DECLARATIONS
Conflict of Interest

The authors have no conflicts to disclose.

Author Contributions

Jun Chai: Conceptualization (lead); Data curation (lead); Formal analysis (lead); Investigation (lead); Methodology (lead); Writing – original draft (lead). **Chen Ming:** Supervision (equal); Validation (equal). **Yi-Yang Sun:** Project administration (lead); Resources (lead); Supervision (lead); Writing – review & editing (lead).

DATA AVAILABILITY

The data that support the findings of this study are available from the corresponding authors upon reasonable request.

REFERENCES

[1] M. Chhowalla, D. Jena, and H. Zhang, Nat. Rev. Mater. **1**(11), 16052 (2016).
[2] I. Ferain, C. A. Colinge, and J.-P. Colinge, Nature **479**(7373), 310–316 (2011).
[3] P. Waltereit, O. Brandt, A. Trampert, H. Grahn, J. Menniger, M. Ramsteiner, M. Reiche, and K. Ploog, Nature **406**(6798), 865–868 (2000).
[4] P. Chen, T. L. Atallah, Z. Lin, P. Wang, S.-J. Lee, J. Xu, Z. Huang, X. Duan, Y. Ping, and Y. Huang, Nature **599**(7885), 404–410 (2021).
[5] S. Sreenivasan, Microsyst. Nanoeng. **3**(1), 17075 (2017).
[6] J. M. Rothberg, W. Hinz, T. M. Rearick, J. Schultz, W. Mileski, M. Davey, J. H. Leamon, K. Johnson, M. J. Milgrew, and M. Edwards, Nature **475**(7356), 348–352 (2011).
[7] X. Wu, W. Gao, J. Chai, C. Ming, M. Chen, H. Zeng, P. Zhang, S. Zhang, and Y.-Y. Sun, Sci. China Mater. **64**(12), 2976–2986 (2021).
[8] S.-H. Wei and S. Zhang, Phys. Rev. B **66**(15), 155211 (2002).
[9] S. Zhang, S.-H. Wei, and A. Zunger, Phys. Rev. Lett. **84**(6), 1232 (2000).
[10] N. Liu, S. E. Rezaei, W. A. Jensen, S. Song, Z. Ren, K. Esfarjani, M. Zebarjadi, and J. A. Floro, Adv. Funct. Mater. **29**(38), 1903157 (2019).
[11] D. McNeill and R. Ware, Br. J. Appl. Phys. **15**(12), 1517 (1964).
[12] C. Giannini, S. Lagomarsino, F. Scarinci, and P. Castrucci, Phys. Rev. B **45**(15), 8822 (1992).
[13] X. Shi and L. Chen, Nat. Mater. **15**(7), 691–692 (2016).
[14] G. Tan, L.-D. Zhao, and M. G. Kanatzidis, Chem. Rev. **116**(19), 12123–12149 (2016).
[15] K. Biswas, J. He, Q. Zhang, G. Wang, C. Uher, V. P. Dravid, and M. G. Kanatzidis, Nat. Chem. **3**(2), 160–166 (2011).
[16] S. Le Tonquesse, Z. Verastegui, H. Huynh, V. Dorcet, Q. Guo, V. Demange, C. Prestipino, D. Berthebaud, T. Mori, and M. Pasturel, ACS Appl. Energy Mater. **2**(12), 8525–8534 (2019).
[17] Z. He, D. Platzek, C. Stiewe, H. Chen, G. Karpinski, and E. Müller, J. Alloys Compd. **438**(1–2), 303–309 (2007).
[18] X. Du, P. Qiu, J. Chai, T. Mao, P. Hu, J. Yang, Y.-Y. Sun, X. Shi, and L. Chen, ACS Appl. Mater. Interfaces **12**(11), 12901–12909 (2020).
[19] P. Qiu, J. Cheng, J. Chai, X. Du, X. Xia, C. Ming, C. Zhu, J. Yang, Y. Y. Sun, and F. Xu, Adv. Energy Mater. **12**(18), 2200247 (2022).
[20] X. Du, P. Hu, T. Mao, Q. Song, P. Qiu, X. Shi, and L. Chen, ACS Appl. Mater. Interfaces **11**(35), 32151–32158 (2019).
[21] P. Rajasekar and A. M. Umarji, Intermetallics **89**, 57–64 (2017).
[22] S. W. Kim, M. Cho, Y. Mishima, and D. Choi, Intermetallics **11**(5), 399–405 (2003).
[23] M. Komabayashi and K.-i. H. Ido, Jpn. J. Appl. Phys., Part 1 **30**(2R), 331 (1991).
[24] J. Chai, C. Ming, X. Du, P. Qiu, Y.-Y. Sun, and L. Chen, Phys. Chem. Chem. Phys. **21**(20), 10497–10504 (2019).

[25]J. P. Perdew, K. Burke, and M. Ernzerhof, Phys. Rev. Lett. **77**(18), 3865 (1996).

[26]G. Kresse and J. Furthmüller, Phys. Rev. B **54**(16), 11169 (1996).

[27]G. Kresse and D. Joubert, Phys. Rev. B **59**(3), 1758 (1999).

[28]H. J. Monkhorst and J. D. Pack, Phys. Rev. B **13**(12), 5188 (1976).

[29]S. Zhang and J. E. Northrup, Phys. Rev. Lett. **67**(17), 2339 (1991).

[30]C. Freysoldt, B. Grabowski, T. Hickel, J. Neugebauer, G. Kresse, A. Janotti, and C. G. Van de Walle, Rev. Mod. Phys. **86**(1), 253 (2014).

[31]C. G. Van de Walle and J. Neugebauer, J. Appl. Phys. **95**(8), 3851–3879 (2004).

[32]X. Wu, C. Ming, J. Shi, H. Wang, D. West, S. Zhang, and Y.-Y. Sun, Chin. Phys. Lett. **39**(4), 046101 (2022).

[33]S. L. Dudarev, G. A. Botton, S. Y. Savrasov, C. Humphreys, and A. P. Sutton, Phys. Rev. B **57**(3), 1505 (1998).

[34]B.-C. Shih, T. A. Abtew, X. Yuan, W. Zhang, and P. Zhang, Phys. Rev. B **86**(16), 165124 (2012).

[35]W. Gao, J. Zhao, and J. R. Chelikowsky, Phys. Rev. Mater. **6**(10), L101402 (2022).

[36]Y. Dusausoy, J. Protas, R. Wandji, and B. Roques, Acta Crystallogr., Sect. B **27**(6), 1209–1218 (1971).

[37]J.-i. Tani and H. Kido, J. Ceram. Soc. Jpn. **109**(1270), 557–560 (2001).

[38]X. Zhao, H. Chen, E. Müller, and C. Drasar, Appl. Phys. A **80**, 1123–1127 (2005).

[39]H. Chen, X. Zhao, C. Stiewe, D. Platzek, and E. Mueller, J. Alloys Compd. **433**(1–2), 338–344 (2007).

[40]M. Ito, H. Nagai, E. Oda, S. Katsuyama, and K. Majima, J. Appl. Phys. **91**(4), 2138–2142 (2002).

30 December 2023 08:25:46